Effects of Multiple Rows and Noncircular Orifices on Dilution Jet Mixing

J.D. Holdeman*
NASA Lewis Research Center, Cleveland, Ohio
and
R. Srinivasan,† E.B. Coleman,‡ G.D. Meyers,§ and C.D. White¶
Garrett Turbine Engine Company, Phoenix, Arizona

This paper presents experimental and empirical model results that extend previous studies of the mixing of single-sided and opposed rows of jets in a confined duct flow to include effects of noncircular orifices and double rows of jets. Analysis of the mean temperature data obtained in this investigation showed that the effects of orifice shape and double rows are significant only in the region close to the injection plane, provided the orifices are symmetric with respect to the main flow direction. Slightly less penetration and mixing is observed for jets from 45-deg slanted slots and the distributions are skewed compared to equivalent-area symmetric orifices. The penetration from two-dimensional slots is similar to that from equivalent-area closely spaced rows of holes, but the mixing is slower for the two-dimensional slots. Calculated mean temperature profiles downstream of jets from noncircular and double rows of orifices, made using an extension of a previous empirical model, are shown to be in good agreement with the measured distributions.

Nomenclature

A_j/A_m = jet-to-mainstream area ratio for each row, $=(\pi/4)/[(S/H_0)(H_0/D)^2]$
AR = orifice aspect ratio (width/length)
C = $(S/H_0)(J)^{0.5}$
C_d = orifice discharge coefficient
D = orifice diameter, $=[(4/\pi)(A_j)]^{0.5}$
D_j = $(D)(C_d)^{0.5}$
DR = jet-to-mainstream density ratio = (T_m/T_j)
dH/dx = duct convergence rate
H_0 = duct height at injection location
H_{eq} = effective duct height, $=H_0$ except for opposed rows of jets with centerlines in line; see Appendix
J = jet-to-mainstream momentum flux ratio $=(DR)(R)^2$
L = width of two-dimensional slot
M = jet-to-mainstream mass flux ratio = $(DR)(R)$
R = jet-to-mainstream velocity ratio = (V_j/U_m)
S = spacing between orifice centers
S_x = spacing between orifice rows
T = temperature
T_j = jet exit temperature
T_m = mainstream temperature
U = velocity
U_m = mainstream velocity
V_j = jet velocity
w_j/w_T = jet-to-total mass flow ratio

$$=\frac{[(DR)(J)]^{0.5}(C_d)(A_j/A_m)}{1+[(DR)(J)]^{0.5}(C_d)(A_j/A_m)}$$

W = width of noncircular orifice
$W^+_{1/2}$ = jet half-width below the centerline (for top injection); see Fig. 4
$W^-_{1/2}$ = jet half-width above the centerline (for top injection); see Fig. 4
x = downstream coordinate, = 0 at injection plane
y = cross-stream coordinate (radial), = 0 at injection wall, $=y_c$ at location of maximum θ in a vertical profile; see Fig. 4
z = lateral coordinate (circumferential), = 0 at centerplane
θ = temperature difference ratio $=(T_m-T)/(T_m-T_j)$; Eq. (1)
θ_c = maximum temperature difference ratio in a vertical profile; see Fig. 4
θ_{EB} = equilibrium θ, $=w_j/w_T$
θ^+_{min} = minimum temperature difference ratio below the centerline (for top injection); see Fig. 4
θ^-_{min} = minimum temperature difference ratio above the centerline (for top injection); see Fig. 4

Presented as Paper 85-1104 at the AIAA/SAE/ASME/ASEE 21st Joint Propulsion Conference, Monterey, CA, July 8-11, 1985; received Feb. 7, 1986; revision received Sept. 10, 1986.

*Senior Research Engineer, Aerothermochemistry Branch. Member AIAA.
†Supervisor, Combustion Engineering Sciences.
‡Senior Engineer, Combustion Engineering Sciences.
§Engineer, Combustion Engineering Sciences.
¶Engineer, Combustion Advanced Technology.

Introduction

THE need to design or tailor the temperature pattern at the combustor exit in gas turbine engines has motivated several investigations on the mixing of jets into a ducted crossflow. These include single and multiple jets injected into a straight duct[1-9] and flow and geometric variations typical of many gas turbine combustors, namely, variable temperature mainstream, flow area convergence, and opposed rows of in-line and staggered jets.[10-15]

Many gas turbine combustors in current operation use multiple (axially staged) rows of dilution jets, some of which use orifice shapes other than circular holes. These were investigated experimentally and analytically in Refs. 16-20 to extend an existing empirical model to include these effects and to increase the available dilution jet data in support of multidimensional numerical modeling.

The combustor dilution zone jet-in-cross flow application is a confined mixing problem, with 10-50% of the total flow entering through the dilution jets. The result is that the average temperature of the exiting flow may differ

significantly from that of the entering mainstream flow. To control or tailor the combustor exit temperature pattern, it is necessary to be able to characterize the exit distribution in terms of the upstream flow and geometric variables. This requires that the entire flowfield be either known or modeled.

From the data of Refs. 1, 11, 14, and 17, an empirical model was developed[4,5] and extended[11,14,17,20] for predicting the temperature field downstream of single and double rows of jets mixing with a confined cross flow. It was shown in Refs. 5 and 18 that this model provides a very good predictive capability for the modeled variables within the parameter range of the generating experiments.

In addition to the evolution and extension of empirical modeling schemes, such as the one used herein, rapid advances have been made recently in the capability of three-dimensional fluid dynamics models and their application to complex flows such as jet(s) in crossflow.[21-25] These codes offer several advantages over empiricism, including the prediction of all flowfield quantities (rather than only those for which empirical models exist), flows outside the range of experiments, or flows where empirical assumptions are known to be invalid.

The three-dimensional codes have been shown[18] to calculate correctly the trends from variation of the independent flow and geometric variables, but they consistently exhibited too little mixing. Although improvements in computational fluid dynamics should provide more quantitative predictions, there would appear to be a continuing need for the empirical model as a near-term design tool.

The present paper presents both measurements and empirical model calculations for configurations with two axially staged rows of jets and single rows of noncircular orifices, including two-dimensional slots. These results also provide a comparison of the mixing of jets from these configurations with those from equivalent area circular orifices. The empirical model presented is shown to provide a good predictive capability for the double-row and noncircular orifice configurations.

Experimental Considerations

Figure 1 shows schematics of the dilution jet flowfield and test rig. Mainstream air was heated to approximately 650 K. Ambient temperature dilution air entered the test section through sharp-edged orifices in the top duct wall of the test section. The orifice plate plenum had the capability to supply independently controlled airflow to each row of jets. The orifice air supply and the main air supply have perforated plates to ensure uniform flow distribution. The several orifice configurations investigated are shown in Fig. 2. The ratio of the orifice plate open area to the mainstream cross-sectional area A_j/A_m was 0.1 for all of the orifice configurations considered, except for the square holes and narrow-slot plates for which $A_j/A_m = 0.05$. The height of the test section H_0 was 10.16 cm and the width 30.48 cm.

The primary independent geometric variables for each row of holes are the spacing between adjacent orifices S and the orifice diameter D; for noncircular orifices, the latter is taken as the diameter of a circle of equal area. The discrete slot orifices investigated had semicircular ends and an aspect ratio (long/short) of 2.8/1. The orifice spacing and equivalent diameter are expressed in dimensionless form as the ratio of the orifice spacing to duct height S/H_0 and the ratio of the duct height to orifice diameter H_0/D. The spacing between rows, S_x/H_0 was 0.5 or 0.25 for the double-row plates tested. For all tests reported herein, the density ratio was approximately equal to 2.2 and the momentum flux ratio varied between ~6-106.

The dilution jet mixing characteristics were determined by measuring mean temperature and pressure distributions with a vertical rake probe, positioned at different axial and lateral stations. This probe had 20 thermocouple elements, with a 20 element total pressure rake and a 20 element static

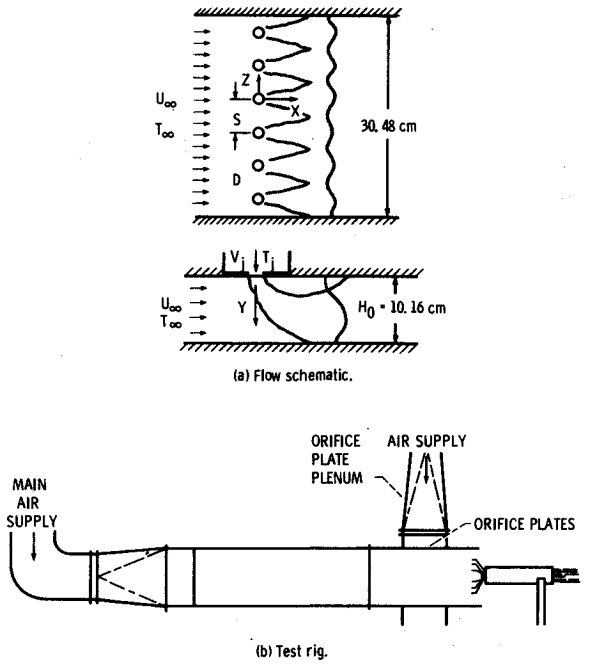

Fig. 1 Schematic of multiple jet flow.

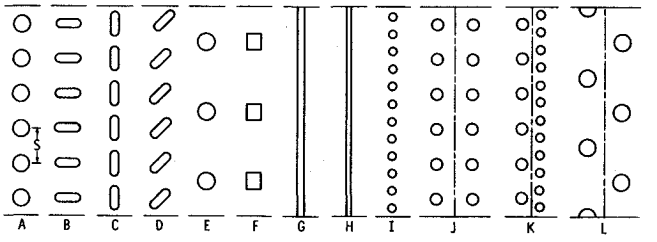

Fig. 2 Orifice configurations.

pressure rake located nominally 5 mm (0.05 H_0) on each side of the thermocouple rake. The center-to-center spacing between sensors on each rake was also 0.05 H_0. The entire probe created less than 3% blockage to the mainstream cross-sectional area. Further details of the experimental set-up and data reduction are given in Refs. 11, 14, and 17. Only temperature measurements are shown here. These were found to be accurate to within 0.2%. Pressure data corresponding to the temperature results shown are given in Ref. 19.

Measured and calculated temperature distributions are presented in this paper in nondimensional form as

$$\theta = \frac{(T_m - T)}{(T_m - T_j)} \tag{1}$$

where T_m is the mainstream temperature, T_j the jet temperature, and T the local temperature. Note that θ equals one if the local temperature is equal to the jet temperature and zero if the local temperature is equal to the mainstream temperature. The equilibrium θ for any configuration θ_{EB} is equal to the fraction of the total flow entering through the dilution jets w_j/w_T.

The temperature field results are presented in three-dimensional oblique views and isotherm contours of the temperature difference ratio θ. A sequence of three-dimensional oblique experimental profiles of this parameter is shown in Fig. 3. In these plots, the temperature distribution is shown in planes normal to the main flow direction. The coordinates Y and Z are, respectively, normal to and along the orifice row in this constant X plane.

The Empirical Flowfield Model

The empirical model for the temperature field downstream of jets mixing with a confined crossflow is based on the observation that properly nondimensionalized vertical temperature profiles everywhere in the flowfield can be expressed in the following self-similar form[5]:

$$\frac{(\theta-\theta^{\pm}_{\min})}{(\theta_c-\theta^{\pm}_{\min})}=\exp\frac{-(\ell n 2)(y-y_c)^2}{(W^{\pm}_{1/2})^2} \qquad (2)$$

where θ is the local temperature difference ratio defined by Eq. (1) and θ_c, $\theta^{-}_{\min}$, $\theta^{+}_{\min}$, $W^{-}_{1/2}$, $W^{+}_{1/2}$, and y_c are scaling parameters as shown in Fig. 4.

Correlations have been developed for each of these in terms of the independent variables J, S/D, H_0/D, Z/S, X/H_0, S_x/H_0, and the mainstream temperature and flow area convergence. The correlations used in the present version of the empirical model are the same as given in Refs. 11, 14, and 17, except that the equations describing the effects of orifice aspect ratio have been modified. The complete set of correlation equations is given in the Appendix.

Although calculations can be performed for most flow and geometric conditions of interest, they will be most reliable for conditions within the range of the experiments on which the correlations are based. These conditions are given in Table 1. The first 10 parameters listed are the independent variables that must be input to the empirical model. Not all combinations of the primary variables in the table were tested; only those combinations that are within the range given for the remaining variables represent conditions that are within the range of the experiments.

Results and Discussion

The following paragraphs and the plots in Figs. 5–10 present the experimental results for single-side injection tests with noncircular orifices and double rows of holes. In addition, the empirical model reported in Ref. 20 has been used to calculate profiles, where applicable, corresponding to the experimental data herein. These are shown in Figs. 11–13. A summary of the test conditions corresponding to the data shown is provided in Table 2.

Slots and Holes

Figure 5 shows three-dimensional oblique θ distributions for equally spaced equivalent-area streamlined, bluff, and slanted slots with $S/H_0=0.5$, $H_0/D=4$ at intermediate momentum flux ratios.

The streamlined slots (Fig. 5a) have deeper jet penetration for $X/H_0<1$ compared to the equivalent area circular holes shown in Fig. 3. Figure 5b shows that, for $X/H_0<1$, jets from bluff slots are more two-dimensional across the orifice centerplane, and their penetration is slightly less, than for circular holes and streamlined slots. Farther downstream, both of the slot configurations and the circular holes produce very similar completely mixed temperature distributions.

Figure 5c shows the temperature distributions that result when the same slot is slanted at 45 deg to the main flow direction. There does not appear to be any advantage in this configuration compared to the circular holes or streamlined or bluff slots; in fact the penetration and mixing are noticeably less. The three-dimensional figures suggest that the asymmetry of the orifices with respect to the main flow direction promotes the development of one vortex of the pair and suppresses the other.

Further insight into the mixing in this case is provided by the isotherm contours in Fig. 6a for circular holes and in Fig. 6b for the 45-deg slanted slots. Note that at the closest downstream location ($X/H_0=0.25$), the isotherms for the flow from the slanted slots are inclined at approximately 45 deg compared to those for jets from circular holes. The influence of the adjacent image vortices in this situation would be to shift the jet centerplanes with increasing downstream distance, as is observed at $X/H_0=0.5$ and 1 in both Figs. 5c and 6b. Comparing the contours at $X/H_0=0.5$ to those at $X/H_0=0.25$ suggests that the distribution has rotated farther as well as shifted, which would follow if the upper vortex (which originated from the trailing edge of the orifice) were stronger than the lower one. This also supports the observation made previously from the oblique plots that the vortices appear to be of unequal strength.

In this study, a single test was performed with the conventional circular holes replaced with squares, to determine the effect of this change in boundary conditions on the profiles. The square orifice was chosen to represent the limiting approximation often made in multidimensional numerical modeling due to limitations on the number of grid nodes available. Figure 7 compares three-dimensional oblique plots of the measured temperature distributions for equivalent-area square and circular holes with $S/H_0=1$ and $H_0/D=4$

Table 1 Range of flow and geometric variables on which the empirical model is based

J	5–105
DR	0.5–2.5
C_d[a]	0.6–0.8
S/H_0	0.125–1
H_0/D	4–16
S_x/H_0	0.25–0.5
X/H_0	0.25–2
Orifice aspect ratio	0.36–2.8
Variable mainstream θ	0–0.5
Duct convergence (dH/dx)	0–0.5
A_j/A_m	0.025–0.1
w_j/w_T	0.075–0.36
$C=(S/H_0)(J^{0.5})$	0.5–10

[a]Not parametrically varied.

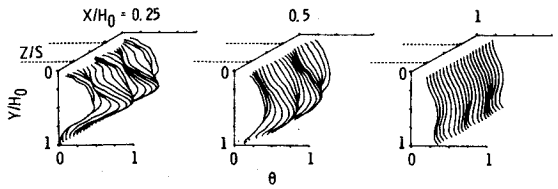

Fig. 3 Experimental mean temperature distributions downstream of jets from round holes in a rectangular duct ($J=26.2$, $S/H_0=0.5$, $H_0/D=4$).

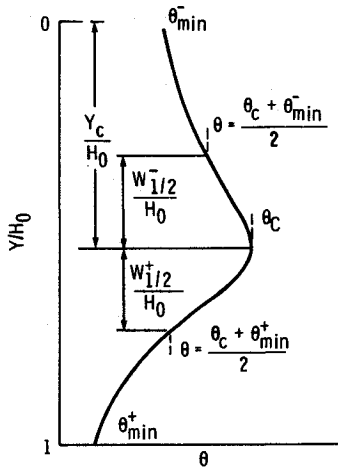

Fig. 4 Schematic of typical vertical temperature profile showing scaling parameters in empirical model.

Table 2 Flow and geometry experimental conditions

Figure	Configuration	Row	S/H_0	H_0/D	A_j/A_m	C_d	DR	J	θ_{EB}[a]	C[b]
3,6a,10a	A: round holes	—	0.5	4.0	0.10	0.76	2.2	26.2	0.36	2.56
5a	B: streamlined slots	—	0.5	4.0	0.10	0.71	2.2	26.5	0.34	2.57
5b	C: bluff slots	—	0.5	4.0	0.10	0.90	2.2	26.6	0.40	2.58
5c,6b	D: slanted slots	—	0.5	4.0	0.10	0.66	2.2	27.1	0.33	2.60
7a	F: square holes	—	1.0	4.0	0.05	0.67	2.1	24.2	0.19	4.92
7b	E: round holes	—	1.0	4.0	0.05	0.67	2.2	23.5	0.19	4.85
8a	G: wide two-dimensional slot	—	—	9.9[a]	0.10	0.76	2.1	6.7	0.22	—
8b	A: round holes	—	0.5	4.0	0.10	0.67	2.1	5.0	0.18	1.19
9a	H: narrow two-dimensional slot	—	—	19.8[c]	0.05	0.72	2.3	105.4	0.35	—
9b	I: round holes	—	0.25	8.0	0.05	0.61	2.3	92.6	0.30	2.60
10b	J: double row	1, 2	0.5	5.7	0.05	0.65	2.2	26.3	0.33	2.56
	in-line		0.5	5.7	0.05	0.65	2.2	26.9		2.59
10c	K: double row	1, 2	0.5	5.7	0.05	0.69	2.2	26.8	0.34	2.59
	dissimilar		0.25	8.0	0.05	0.70	2.2	26.6		1.29
10d	L: double row	1, 2	1.0	4.0	0.05	0.65	2.2	26.8	0.33	5.18
	staggered		1.0	4.0	0.05	0.68	2.2	26.7		5.18

[a] $\theta_{EB} = w_j/w_T$. [b] $C = (S/H_0)(J^{0.5})$. [c] H_0/L.

at intermediate momentum flux ratios. The mean temperature field for these configurations is nearly identical at all downstream distances.

A limited number of tests were performed with two-dimensional slots in place of the discrete jets primarily for comparison with the temperature distributions measured downstream of closely spaced equivalent-area holes. Figures 8a and 9a show the results respectively, for a wide two-dimensional slot ($A_j/A_m = 0.1$) at a low momentum flux ratio and a narrower two-dimensional slot ($A_j/A_m = 0.05$) at a high momentum flux ratio. Distributions for closely spaced ($S/D = 2$) circular holes with equal area and similar momentum flux ratios are shown in Figs. 8b and 9b and centerplane profiles for the circular jet case and the slot profile are shown in Figs. 8c and 9c.

The similarity in the penetration shown by these profiles is surprising, since the two-dimensional slot flow completely blocks the mainstream on the injection side of the duct, whereas the discrete jet flow is highly three-dimensional in that the mainstream flow is deflected around as well as over the jets, creating the well-known vortex pair and kidney-shaped mixing pattern. The increased blockage in the slot-jet cases results in less mixing and the temperature difference ratios in the wake region of these flows are significantly higher than in the wake of the jets from circular holes.

Experimental profiles for the narrow slot at an intermediate momentum flux ratio (shown in Ref. 14) are similar to those shown in Fig. 8a for the wide slot at a low momentum flux ratio and profiles for the wide slot at an intermediate momentum flux ratio[14] are similar to those shown in Fig. 9a for the narrow slot at a high momentum flux ratio. The corresponding circular hole cases are also similar, as would be expected since the values of $C = (S/H_0)(J^{0.5})$ are similar,[13,18] but the similarity of the corresponding two-dimensional slot profiles was not expected.

Double Rows of Holes

Figure 10 shows three-dimensional oblique and isotherm contour plots at intermediate momentum flux ratios and $X/H_0 = 0.5$ for jets from a single row of equally spaced circular orifices and jets from equivalent-area double rows of circular orifices. The single row (configuration A in Fig. 2 and Table 2) is shown in Fig. 10a; two rows of jets with centerlines in-line (configuration J) are shown in Fig. 10b; two rows of jets with a different hole size and spacing in each row (configuration K) are shown in Fig. 10c; and a staggered double-row (configuration L) is shown in Fig. 10d. For the double row configurations, $X/H_0 = 0$ was taken to be midway between the rows.

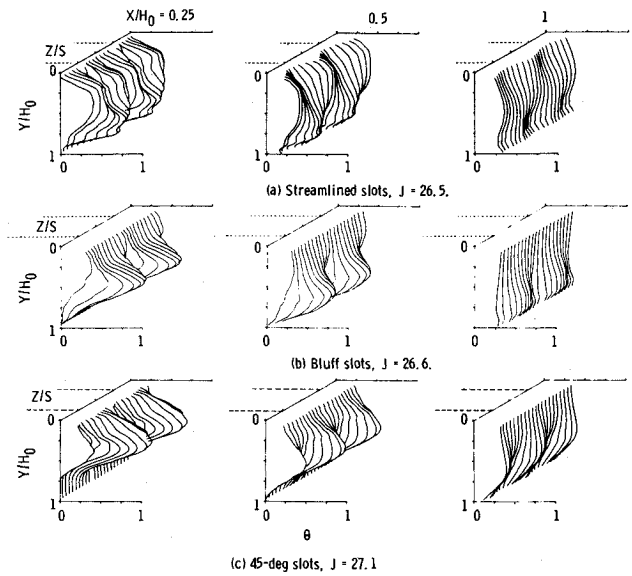

Fig. 5 Comparison of three-dimensional oblique temperature distributions downstream of jets at intermediate momentum flux ratios from equivalent-area streamlined, bluff, and slanted slots ($S/H_0 = 0.5$, $H_0/D = 4$).

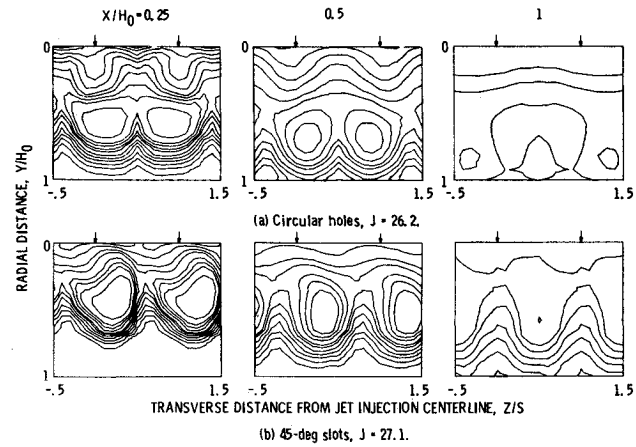

Fig. 6 Comparison of isotherm contours downstream of jets at intermediate momentum flux ratios from round holes and 45-deg slanted slots ($S/H_0 = 0.5$, $H_0/D = 4$).

The temperature distributions for the double in-line rows are strikingly similar to that for the single row, as was also seen in Ref. 1. The double row of dissimilar holes gives a similar distribution also and shows the dominance of the lead row in establishing the jet penetration and first-order profile shape.

The influence of the leading row on the temperature field is also evident in Fig. 10d, where the distribution from a double row of staggered jets at an intermediate momentum flux ratio is shown for comparison with the other configurations. The jets from the leading row penetrate farther across the duct than do those from the single row, as would be expected due to the larger spacing (cf. Refs. 2, 9, and 13). The penetration of the jets in the trailing row is suppressed, presumably by the vortex field of the lead row. Farther downstream, the temperature fields from the double row of staggered jets were found to be similar to those from the single row and the other double-row configurations.

Empirical Model Results

Figure 11 shows a sequence of three-dimension oblique profiles for top injection of a single row of jets into a straight duct that were calculated using the empirical model given by Eq. (2) and the Appendix. The conditions for this case are nearly identical to those for which experimental profiles are shown in Fig. 3. The empirical model agrees very well with the data in this case as shown also in Ref. 18, as the flow centerline is near the center of the duct, and all of the measured vertical profiles are consistent with the shape assumption in the empirical model.

Calculated profiles for streamlined, bluff, and slanted slots are shown in Fig. 12. This figure is directly comparable to Fig. 5. The principal effects seen in the experimental data are also evident in the empirical model calculations, except for the asymmetry about the flow centerplane in the case of the slanted slots. The streamlined and bluff slots were modeled by substituting the ratio of the orifice spacing to slot width (S/W) for the orifice spacing to diameter ratio (S/D) in the correlations. The slanted slots were modeled with distributions for circular holes shifted laterally as a function of momentum flux ratio and downstream distance.

Figure 13 shows calculated profiles for the several double-row configurations examined. The profiles at $X/H_0 = 0.5$ are comparable to those for the in-line, dissimilar, and staggered configurations in Figs. 10b–10d. All the empirical calculations result from a superposition of independent calculations of the two rows. This technique works very well in the case of in-line holes, is acceptable for rows with different size holes, and is less accurate for staggered jets, since the suppression of the trajectory of the trailing row is not modeled.

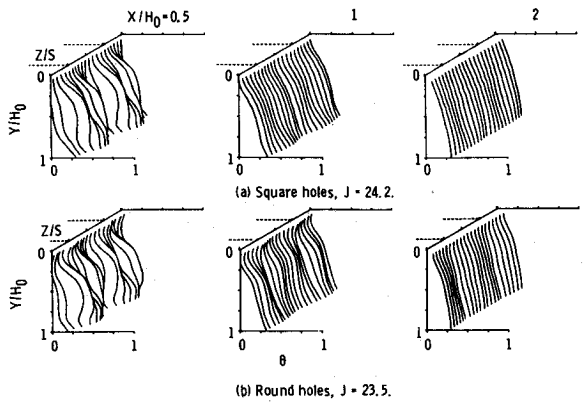

Fig. 7 Comparison of temperature distributions downstream of jets at intermediate momentum flux ratios from square and round holes ($S/H_0 = 1$, $H_0/D = 4$).

Limitations and Applicability

Examination of the empirical model results in Ref. 18 shows that correlation of experimental data can provide a good predictive capability within the parameter range of the generating experiments, provided that the experimental results are consistent with the assumptions made in the empirical model. These models must, however, be used with caution, or not at all, outside this range.

Previous experimental and analytical results[5,13,18] have shown the importance of coupling the orifice spacing and momentum flux ratio on profile shape and location. Namely,

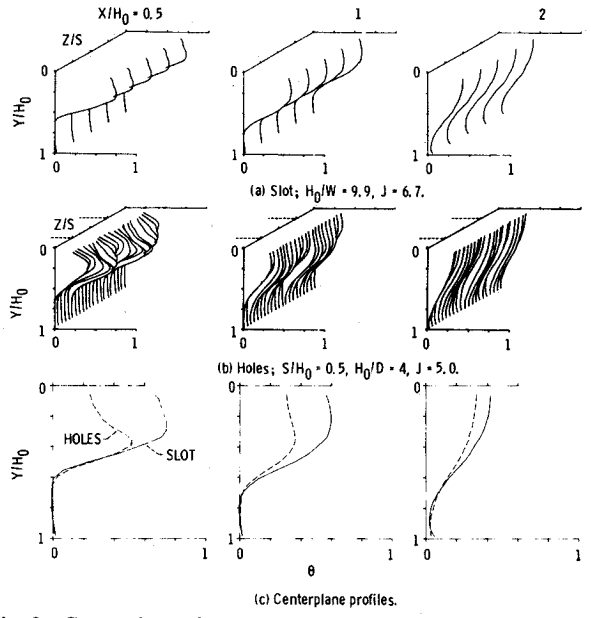

Fig. 8 Comparison of temperature distributions downstream of jets at low momentum flux ratios from a wide two-dimensional slot and closely spaced round holes ($A_j/A_m = 0.1$).

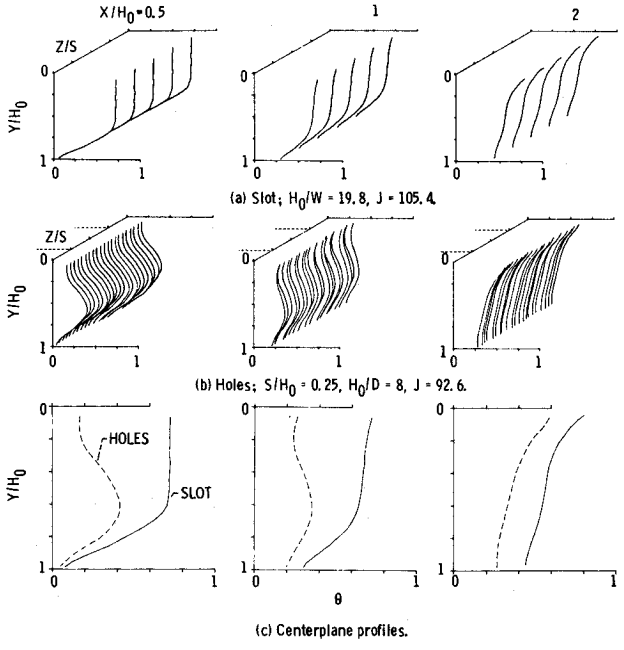

Fig. 9 Comparison of temperature distributions downstream of jets at high momentum flux ratios from a narrow two-dimensional slot and closely spaced round holes ($A_j/A_m = 0.05$).

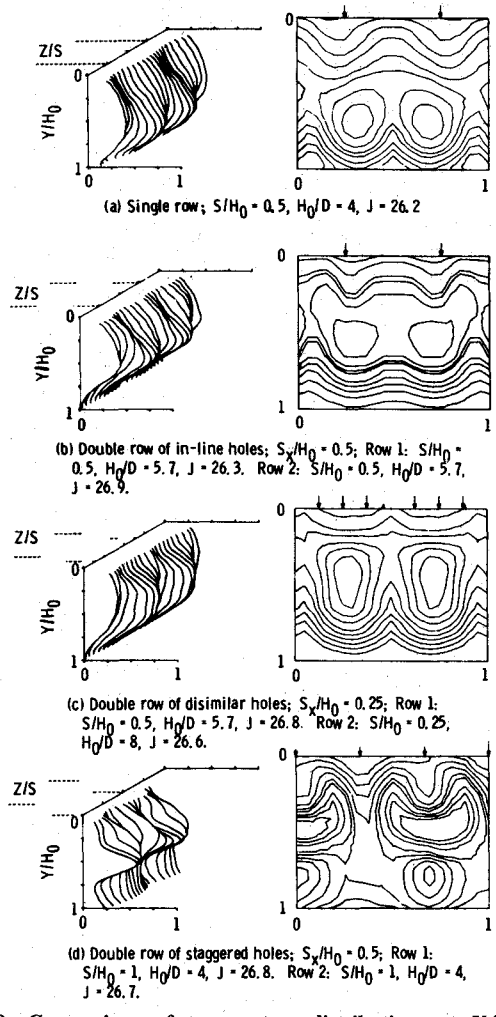

Fig. 10 Comparison of temperature distributions at $X/H_0 = 0.5$ downstream of jets at intermediate momentum flux ratios from double and single rows of holes ($A_j/A_m = 0.1$).

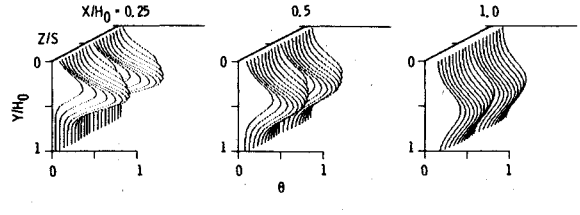

Fig. 11 Calculated temperature profiles for top injection from round holes in a rectangular duct ($S/H_0 = 0.5$, $H_0/D = 4$, $J = 26.4$, $C_d = 0.64$).

profiles are similar for equal values of C, where $C = (S/H_0)(J^{0.5})$. In general, the empirical model provides good temperature field predictions for single-side injection when $1 < C < 5$. Similarly, good predictions are obtained for opposed in-line jets provided that $0.5 < C < 2.5$. For opposed rows of staggered jets, satisfactory profiles were obtained with C approximately equal to 5; but it was shown in Ref. 14 that opposed staggered jets with lower values of C were modeled better using correlations for the opposed in-line case. The experimental profiles for conditions giving optimum mixing in opposed staggered-jet configurations are somewhat at variance with the model assumptions. Although the agreement between the data and model calculations is satisfactory in these cases, the model should be used only as a first-order tool to aid existing design methods.

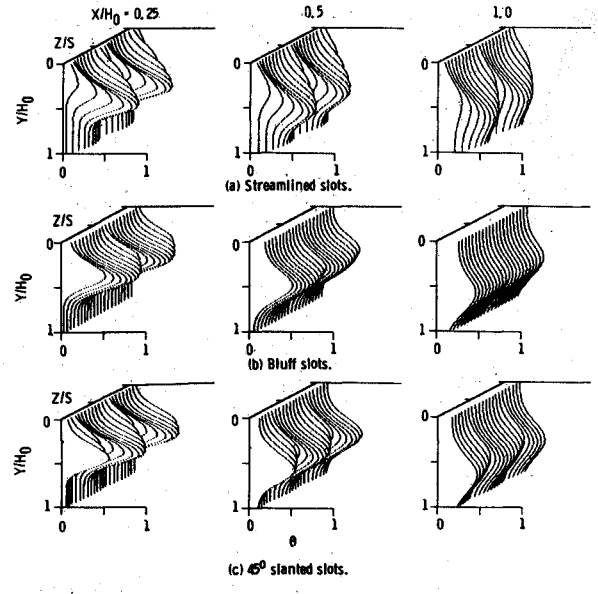

Fig. 12 Calculated temperature profiles for streamline, bluff, and slanted slots [$\mathcal{R}$(long:short) = 2.8:1, $S/H_0 = 0.5$, $H_0/D = 4$, $J = 26.4$, $DR = 2.2$, $C_d = 0.64$].

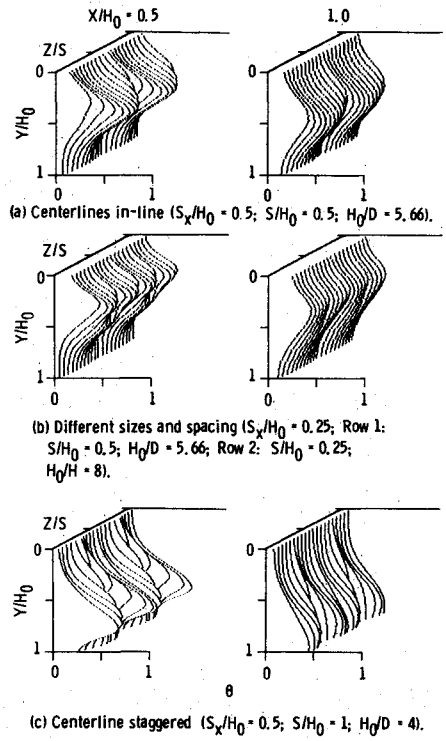

Fig. 13 Calculated temperature profiles for double rows of jets, with downstream distance measured from midway between rows ($J = 26.4$, $DR = 2.2$, $C_d = 0.64$).

The technique of superposing independent calculations is reasonably successful in approximating the flowfields for double rows of jets and jets downstream of nonisothermal mainstream profiles. There are, however, features in these flows that this technique cannot model, as suggested here and in Ref. 18. It should also be noted that the form of the empirical correlations in the current model (and previous versions used in Refs. 4, 5, 9, 11, 14, 17, and 18) precludes their use for semiconfined flows (large H_0/D or S/D), single-jet flows, or flows in which it is known a priori that the primary assumptions in the model will be invalid.

Summary of Results

From analyses of the experimental data and empirical profiles for one-side injection through noncircular and double rows of sharp-edged orifices, it was concluded that:

1) For orifices that are symmetric with respect to the main flow direction, the effects of shape are significant only in the region close to the injection plane. In regions beyond $X/H_0 = 1$ $(X/D) \geq 4$ for the orifices tested, the temperature distributions are similar to those from equally spaced, equivalent-area circular orifices.

2) The penetration and mixing of 45 deg slanted slots are less than for streamlined or bluff slots or equivalent-area circular holes and the temperature distributions are skewed and shift laterally with respect to the injection centerplane.

3) Jet penetration for two-dimensional slots is similar to the centerplane value for closely spaced $(S/D=2)$, equivalent-area holes, but the temperature difference ratios, particularly in the wake region, indicate that the mixing is slower in the two-dimensional slot cases.

4) At the same momentum flux ratio, and with the same S/H_0 in (at least) the lead row, double rows of jets have temperature distributions similar to those from a single row of equally spaced, equivalent-area circular orifices.

5) The temperature distributions for streamlined and bluff slots can be satisfactorily modeled by substituting the ratio of the orifice spacing to orifice width (S/W) for the ratio of the orifice spacing to orifice diameter (S/D) in the correlation equations.

6) The temperature field for slanted slots can be approximated by laterally shifting profiles calculated for a row of circular orifices.

7) The temperature field for axially staged rows of jets can be modeled by superimposing independent calculations of the temperature distributions due to each individual row of jets.

Appendix: Correlation Equations

Primary parameter given in the following equations are shown in Fig. 4.

Jet Thermal Centerline Trajectory

$$Y_c/H_{eq} = (a_1)(0.3575)(J)^{0.25}(S/D)^{0.14}(H_{eq}/D)^{-0.45} \times (C_d)^{0.155}(X/H_{eq})^{0.17}[\exp(-b)]$$

where

$$a_1 = \min[(1+S/H_{eq}), 2]$$

$$b = (0.091)(X/H_{eq})^2[(H_{eq}/S) - (J^{0.5})/3.5)]$$

Centerplane Maximum Temperature Difference Ratio

$$\theta_c = \theta_{EB} + (1-\theta_{EB})[(a_1)(J)^{-0.35}(C_d)^{0.5}(H_{eq}/D)^{-1} \times (X/H_{eq})^{-1}]^f$$

where

$$f = 1.15[(S/H_{eq})/(1+S/H_{eq})]^{0.5}$$

$$\theta_{EB} = w_j/w_T$$

Centerplane Minimum Temperature Difference Ratios

Opposite side of centerline

$$(\theta^+_{min})/(\theta_c) = 1 - \exp(-c^+)$$

where

$$c^+ = (a_3)(0.038)(J)^{1.62}(S/D)^{1.5}(H_{eq}/D)^{-2.57} \times (C_d)^{0.535}(X/H_{eq})^{1.1}$$

$$a_3 = 1 \quad \text{if } (Y_c/H_{eq} + W^+_{1/2}/H_{eq}) \leq 1$$

$$a_3 = (H_0/H_{eq})^{3.67} \quad \text{if } (Y_c/H_{eq} + W^+_{1/2}/H_{eq}) > 1$$

Injection side of centerline

$$(\theta^-_{min})/(\theta_c) = 1 - \exp(-c^-)$$

where

$$c^- = (Q)(1.57)(J)^{-0.3}(S/D)^{-1.4}(H_{eq}/D)^{0.9} \times (C_d)^{0.25}(X/H_{eq})^{0.9}$$

$$Q = 1 \quad \text{if } (Y_c/H_{eq} + W^+_{1/2}/H_{eq}) \leq 1$$

$$Q = \exp[(0.22)(X/H_{eq})^2((J^{0.5})/5 - S/H_{eq})] \quad \text{if } (Y_c/H_{eq} + W^+_{1/2}/H_{eq}) > 1$$

Centerplane Half-Widths

Opposite side of centerline

$$(W^+_{1/2})/H_{eq} = (0.1623)(J)^{0.18}(S/D)^{-0.25}(H_0/H_{eq})^{0.5} \times (C_d)^{0.125}(X/H_{eq})^{0.5}$$

Injection side of centerline

$$(W^-_{1/2})/H_{eq} = (0.2)(J)^{0.15}(S/D)^{0.27}(H_{eq}/D)^{-0.38} \times (H_0/H_{eq})^{0.5}(C_d)^{0.055}(X/H_{eq})^{0.12}$$

Off-Centerplane Thermal Trajectory

$$Y_{c,z}/Y_c = 1 - (4)(Z/S)^2[\exp(-g)]$$

where

$$g = (0.227)(J)^{0.67}(S/D)^{-1}(H_{eq}/D)^{0.54}(C_d)^{0.23} \times (X/H_{eq})^{0.54}$$

Off-Centerplane Maximum Temperature Difference Ratio

$$\theta_{c,z}/\theta_c = 1 - (4)(Z/S)^2\exp(-d)$$

where

$$d = (0.452)(J)^{0.53}(S/D)^{-1.53}(H_{eq}/D)^{0.83}(C_d)^{0.35} \times (X/H_{eq})^{0.83}$$

Off-Centerplane Minimum Temperature Difference Ratios

$$\theta^{\pm}_{min,z}\theta_{c,z} = \theta^{\pm}_{min}\theta_c$$

Off-Centerplane Half-Widths

$$W^{\pm}_{1/2,z}/H_{eq} = W^{\pm}_{1/2}/H_{eq}$$

The six scaling parameters, Y_c/H_{eq}, θ_c, θ^+_{min},θ^-_{min}, $W^+_{1/2}/H_{eq}$, and $W^-_{1/2}/H_{eq}$, are used in Eq. (2) to define the vertical profile at any x,z location in the flow. For all except the case of opposed rows of jets with centerlines in-line, H_{eq} in the correlation equations is equal to H_0, the height of the duct at the injection location.

Nonisothermal Mainstream Double (Axially Staged) Rows of Jets Opposed Rows of Jets with Centerlines Staggered

It was shown in Ref. 18 that these flows can be satisfactorily modeled by superimposing independent calculations of the separate elements. This is accomplished as follows:

$$\theta = [\theta_1 + \theta_2 - (2)(\theta_1)(\theta_2)] / [1 - (\theta_1)(\theta_2)]$$

Note that $\theta = \theta_1$ at any location where $\theta_2 = 0$ (and $\theta = \theta_2$ if $\theta_1 = 0$); and that $\theta \leq 1$ (provided that θ_1 and θ_2 are each ≤ 1). Also, for the completely mixed case θ_{EB} is equal to the ratio of the total jet flow to the mainstream flow as required.

Opposed Rows of Jet with Centerlines In-line

It was observed in Ref. 3 that the flowfield downstream of opposed jets was similar to that downstream of a single jet injected toward an opposite wall at half the distance between the jets. This is confirmed by the experimental results in Ref. 14 also. Thus, for the symmetric case, $H_{eq} = H_0/2$.

In general, these flows can be modeled by calculating an effective duct height as proposed in Ref. 12, namely,

$$[H_{eq}]_{top} = (H_0) \frac{[(A_j/A_m)(J^{0.5})]_{top}}{[(A_j/A_m)(J^{0.5})]_{top} + [(A_j/A_m)(J^{0.5})]_{bottom}}$$

and

$$[H_{eq}]_{bottom} = H_0 - (H_{eq})_{top}$$

Flow Area Convergence

This case is modeled by assuming that the accelerating mainstream will act to decrease the effective momentum flux ratio as the flow proceeds downstream; thus,

$$J(x) = (J)[H(x)/H_0]^2$$

Note that the trajectory and the jet half-widths are calculated in terms of the duct height at the injection location and so must be scaled by the inverse of the convergence rate, $H_0/H(x)$, to give profiles in terms of the local duct height.

Orifice Aspect Ratio

It was observed in Ref. 17 that bluff slots resulted in slightly less jet penetration and more two-dimensional profiles than circular holes and that streamlined slots resulted in slightly greater jet penetration and more three-dimensional profiles. This effect is modeled by using the ratio of the orifice spacing to the orifice width S/W in lieu of S/D in the correlation equations. For rectangular orifices with circular ends,

$$S/W = (S/D)[1 + (4/\pi)(AR - 1)]^{0.5} \quad \text{if } AR > 1$$

and

$$S/W = (S/D)[1 + (4/\pi)(1/AR - 1)]^{0.5}/AR \quad \text{if } AR < 1$$

where only $AR = W/L$.

Slanted Slots

Two effects were noted in the experimental results for slanted slots, namely, that the centerplanes shifted laterally with increasing downstream distance and the axes of the kidney-shaped temperature contours were inclined with respect to the injection direction. The former is modeled as a function of momentum flux ratio and downstream distance as

$$dZ/S = \sin[(\pi/2)(a)]$$

where $a = \min[1, (X/H_{eq})(J/26.4)^{0.25}]$.

The rotation effect observed in the experimental data is not modeled.

References

[1] Walker, R.E. and Kors, D.L., "Multiple Jet Study Final Report," NASA CR-121217, June 1973.

[2] Holdeman, J.D., Walker, R.E., and Kors, D.L., "Mixing of Multiple Dilution Jets with a Hot Primary Airstream for Gas Turbine Combustors," AIAA Paper 73-1249, Nov. 1973 (NASA TM X-71426).

[3] Kamotani, Y. and Greber, I., "Experiments on Confined Turbulent Jets in Cross Flow," NASA CR-2392, March 1974.

[4] Walker, R.E. and Eberhardt, R.G., "Multiple Jet Study Data Correlations," NASA CR-134795, April 1975.

[5] Holdeman, J.D. and Walker, R.E., "Mixing of a Row of Jets with a Confined Crossflow," *AIAA Journal*, Vol. 15, Feb. 1977, pp. 243-249 [see also AIAA Paper 76-48 (NASA TM-71787)].

[6] Cox, G.B. Jr., "Multiple Jet Correlations for Gas Turbine Engine Combustor Design," *Journal of Engineering for Power*, Vol. 98, No. 2, April 1976, pp. 265-273.

[7] Cox, G.B. Jr., "An Analytical Model for Predicting Exit Temperature Profile from Gas Turbine Engine Annular Combustors," AIAA Paper 75-1307, Sept. 1975.

[8] Khan, Z.A., McGuirk, J.J., and Whitelaw, J.H., "A Row of Jets in Crossflow," *Fluid Dynamics of Jets with Application to V/STOL*, AGARD-CP-308, 1982, Paper 10.

[9] Holdeman, J.D., "Perspectives on the Mixing of a Row of Jets with a Confined Crossflow," AIAA Paper 83-1200, June 1983 (NASA TM-83457).

[10] Atkinson, K.N., Khan, Z.A., and Whitelaw, J.H., "Experimental Investigation of Opposed Jets Discharging Normally into a Crossstream," *Journal of Fluid Mechanics*, Vol. 115, 1982, pp. 493-504.

[11] Srinivasan, R., Berenfeld, A., and Mongia, H.C., "Dilution Jet Mixing Program Phase I Report," Garrett Turbine Engine Co., Phoenix, AZ, Rept. 21-4302, Nov. 1982 (also NASA CR-168031).

[12] Wittig, S.L.K., Elbahar, O.M.F., and Noll, B.E., "Temperature Profile Development in Turbulent Mixing of Coolant Jets with a Confined Hot Cross-Flow," *Journal of Engineering for Gas Turbines and Power*, Vol. 106, 1984, p. 1983 (see also ASME Paper 83-GT-39).

[13] Holdeman, J.D., Srinivasan, R., and Berenfeld, A., "Experiments in Dilution Jet Mixing," *AIAA Journal*, Vol. 22, Oct. 1984, pp. 1436-1443 [see also AIAA Paper 83-1201 (NASA TM 83457)].

[14] Srinivasan, R., Coleman, E., Johnson, K., and Mongia, H.C., "Dilution Jet Mixing Program Phase II Report," Garrett Turbine Engine Co., Phoenix, AZ, Rept. 21-4804, June 1984 (NASA CR-174624).

[15] Holdeman, J.D. and Srinivasan, R., "Modeling of Dilution Jet Flowfields," *Combustion Fundamentals Research*, NASA CP-2309, April 1984, pp. 175-187.

[16] Holdeman, J.D., Srinivasan, R., Coleman, E.B., Meyers, G.D., and White, C.D., "Experiment in Dilution Jet Mixing-Effects of Multiple Rows and Non-circular Orifices," AIAA Paper 85-1104, July 1985 (NASA TM-86996).

[17] Srinivasan, R., Coleman, E., Meyers, G., and White, C., "Dilution Jet Mixing Program Phase III Report," Garrett Turbine Engine Co., Phoenix, AZ, Rept. 21-5418, Sept. 1985 (NASA CR-174884).

[18] Holdeman, J.D. and Srinivasan, R., "Modeling of Dilution Jet Flowfields," *Journal of Propulsion and Power*, Vol. 2, Jan./Feb. 1986, pp. 4-10 [see also AIAA Paper 84-1379 (NASA TM 83708)].

[19] Srinivasan, R. and White, C., "Dilution Jet Mixing Program Supplementary Report," Garrett Turbine Engine Co., Phoenix, AZ, Rept. 21-5705, March 1986 (NASA CR-175043).

[20] Holdeman, J.D. and Srinivasan, R., "Perspectives on Dilution Jet Mixing," AIAA Paper 86-1611, June 1986 (NASA TM 87294).

[21] Bruce, T.W., Mongia, H.C., Reynolds, R.S., "Combustor Design Criteria Validation," AiResearch Manufacturing Co. of Arizona, Phoenix, AZ, Rept. 75-211682(38), March 1979 (USARTL-TR-78-55A, B, and C).

[22] Claus, R.W., "Analytical Calculation of a Single Jet in Crossflow and Comparison with Experiment," AIAA Paper 83-0238, Jan. 1983 (NASA TM-83027).

[23] Sturgess, G.J., "Aerothermal Modeling Phase I Final Report," Pratt & Whitney Aircraft, East Hartford, CT, Rept. PWA-5907-19, May 1983 (NASA CR-168202).

[24] Srinivasan, R., Reynolds, R., Ball, I., Berry, R., Johnson, K., and Mongia, H.C., "Aerothermal Modeling Program: Phase I Final Report—Vol. 2" Garrett Turbine Engine Co., Phoenix, AZ, Rept. 21-4742-2, Aug. 1983 (NASA CR-168243).

[25] Kenworthy, M.J., Correa, S.M., and Burrus, D.L., "Aerothermal Modeling Phase I—Final Report: Vol. I—Model Assessment," NASA CR-168296, Vol. 1, Nov. 1983.